

Supporting Information

Robust and broadband optical coupling by topological waveguide arrays

Wange Song^{1,3}, Wenzhao Sun², Chen Chen^{1,3}, Qinghai Song², Shumin Xiao^{2*}, Shining Zhu^{1,3}, and Tao Li^{1,3*}

S1. Simulation and analysis details on topological DC and BS designs

A commercial finite-element analysis solver (Comsol Multiphysics 5.3) was employed for full-wave simulations. The individual silicon waveguide on the sapphire substrate supports a fundamental mode with a propagation constant $\beta_0=2.16k_0$ (k_0 is the wave vector in free space) at wavelength of 1550 nm. Here, the waveguide is defined as width of $w=400$ nm and height of $h=220$ nm. **Figure S1a** shows the coupling coefficient as the function of gap distance, where two gap distances are selected for our SSH modeled waveguide array, *i.e.*, $d_1=200$ nm for $c_1=0.020k_0$ and $d_2=120$ nm for $c_2=0.037k_0$.

To demonstrate the influence of the structure parameters on the TES property, we calculated a series of structures by varying c_2 (with a fixed c_1) and waveguide number N . Then, the coupling coefficients (κ_{DC} and κ_{BS}) of TES modes in DC and BS devices can be worked out as diagrams with respect to the dimerization $\delta=|c_2-c_1|$ and waveguide number N , as shown in Figure S1c,d respectively. According to these data, the coupling length can be deduced (e.g., $L_{DC}=\pi/2\kappa_{DC}$). In our work, we take the 6 waveguides for the DC device and 11 for BS, and the coupling lengths are calculated as the function of δ , as shown in Figure S1b. It is obtained of $L_{DC}=89.7$ μm and $L_{BS}=70.6$ μm , according to the designed $d_2=120$ nm with $c_2=0.037k_0$.

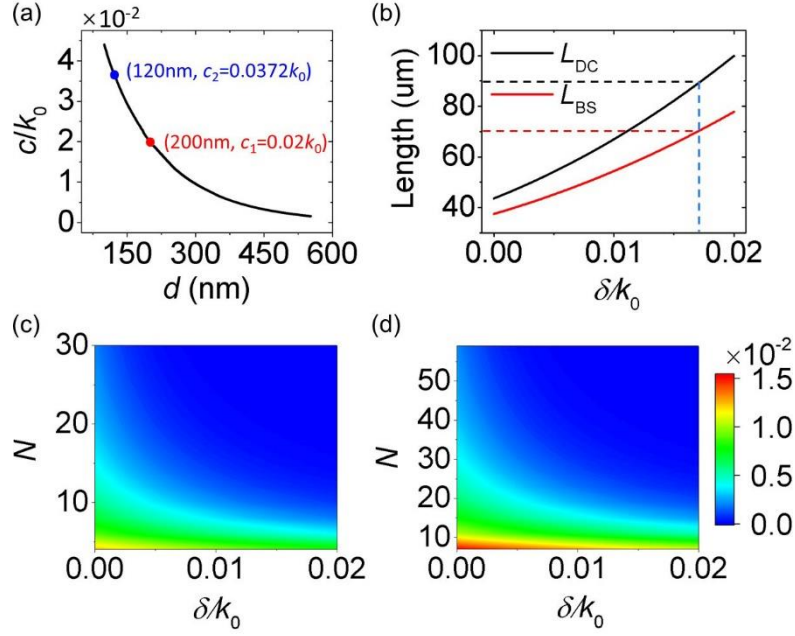


Figure. S1. Simulation and analysis details on topological DC and BS. (a) Coupling coefficient c/k_0 as a function of gap d with $w=400$ nm and $h=220$ nm, where two dots indicate what we selected in our modeling. (b) Coupling distance L with respect to δ/k_0 with $N=6$ for topological DC and $N=11$ for topological BS. (c,d) Diagram of coupling strength (κ/k_0) of the TES with respect to the waveguide number N and the dimerization δ/k_0 for (c) topological DC and (d) topological BS.

S2. Controlled samples with structural discrepancies and detailed experimental data

In experiments, the random disorders are generated by the fabrications with deviations ~ 12 nm in both waveguide gaps and widths. To guarantee the largest deviation degree (η) for corresponding fluctuation strengths, other discrepancies were also artificially introduced in several randomly selected waveguides gaps with a maximum Δd of 10 nm, 20 nm, 30 nm and 40 nm (corresponding to $\eta=8.3\%$, 16.7% , 24.9% , and 33.2%). In comparison, we also designed the conventional DC/BS devices composed of two/three coupled waveguides, where the ideal one (without discrepancy) is of $d=410/440$ nm for a coupling length of $100/80$ μm to keep the same as the experimental topological

DC/BS. Discrepancies of $\Delta d_{\max}=20$ nm, 40 nm, 60 nm and 80 nm were introduced (corresponding to $\eta=4.9\%$, 9.8% , 14.7% , and 19.6%) for conventional DC, and $\Delta d_{\max}=10$ nm, 20 nm, 40 nm, 60 nm, and 80 nm (corresponding to $\eta=2.3\%$, 4.6% , 9.2% , 13.8% , and 18.4%) for conventional BS.

Here, we take a careful inspection on the array samples, as their SEM images shown in **Figure S2**, for the ideal and deviated DC devices. Figure S2a is the ideal structure with designed alternating gaps ($d_1=200$ nm and $d_2=120$ nm). However, it is not “ideal” enough, and there are about 1.6~2.5 nm discrepancies after the very fine fabrication. As for the controlled samples, besides the randomly artificially introduced maximum Δd for various parameters η , there are still additional random discrepancies introduced in fabrication, see Figure S2b,c for the $\eta=8.3\%$ ($\Delta d_{\max}=10$ nm) and $\eta=16.7\%$ ($\Delta d_{\max}=20$ nm) cases, respectively, where all the waveguides are affected and disorders exist across all the structure (*i.e.*, one of the samples with $\eta=8.3\%$ has discrepancies of $\Delta d_1=-6.1$ nm, $\Delta d_2=7.8$ nm, $\Delta d_3=-7.8$ nm, $\Delta d_4=5.3$ nm, and $\Delta d_5=-12.0$ nm, as shown in Figure S2b). These fabrication errors may even enlarge the controlled ones (*e.g.*, $\Delta d \approx 23.2$ nm for the gap of 96.8 nm in Figure S2c). **Figure S3** shows the coupling ratio as a function of absolute disorders (Δd_{\max}) for topological and conventional devices. Detailed experimental data for more samples with disorders is shown here in **Figure S4**.

It should be mentioned that current complementary metal-oxide-semiconductor (CMOS) technique has been well developed and the 5 nm critical dimension has been achieved. However, the device cost is always a critical issue. Typically, the cost for the same chip can be orders of magnitude lower when it was fabricated with a 40 nm CMOS technology instead of 5 nm CMOS technology. In this sense, it is not only necessary but also highly desirable to increase the fabrication tolerance. Better tolerance means that the photonic chips can be produced with a less time or lower cost. Meanwhile, the current CMOS technology typically works well for Si, Si_3N_4 , TiO_2 , and III-V semiconductors. But the new photonic design by the application of TES in integrated photonics, which is of general sense and importance in photonic designs and will not be limited to silicon

platform. It is easy to extend to other material systems (i.e. Lithium niobate based photonic circuit), where the fabrication is still difficult currently. More importantly, here we provided a new method to access the robust coupling that was never revealed before, and promises a general significance in applying the topological design to optical integrations.

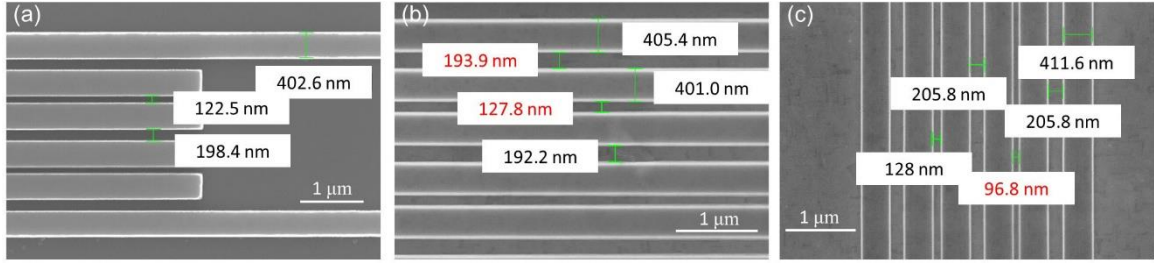


Figure S2. SEM images of fabricated samples. (a) The ideal SSH design of topological DC. (b) The discrepancy of $\eta=8.3\%$ ($\Delta d_{\max}=10$ nm), and (c) discrepancy of $\eta=16.7\%$ ($\Delta d_{\max}=20$ nm), marked with actual structural parameters, where the red markers are randomly artificially introduced maximum discrepancies. It is clearly seen the fabrication errors besides the intentionally introduced discrepancies.

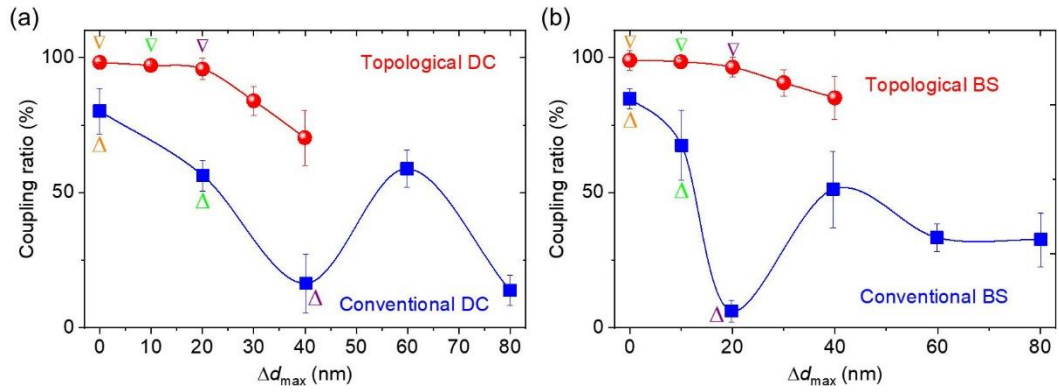


Figure S3. The coupling ratio as a function of absolute disorders. (a) Topological and conventional DC devices. (b) Topological and conventional BS devices.

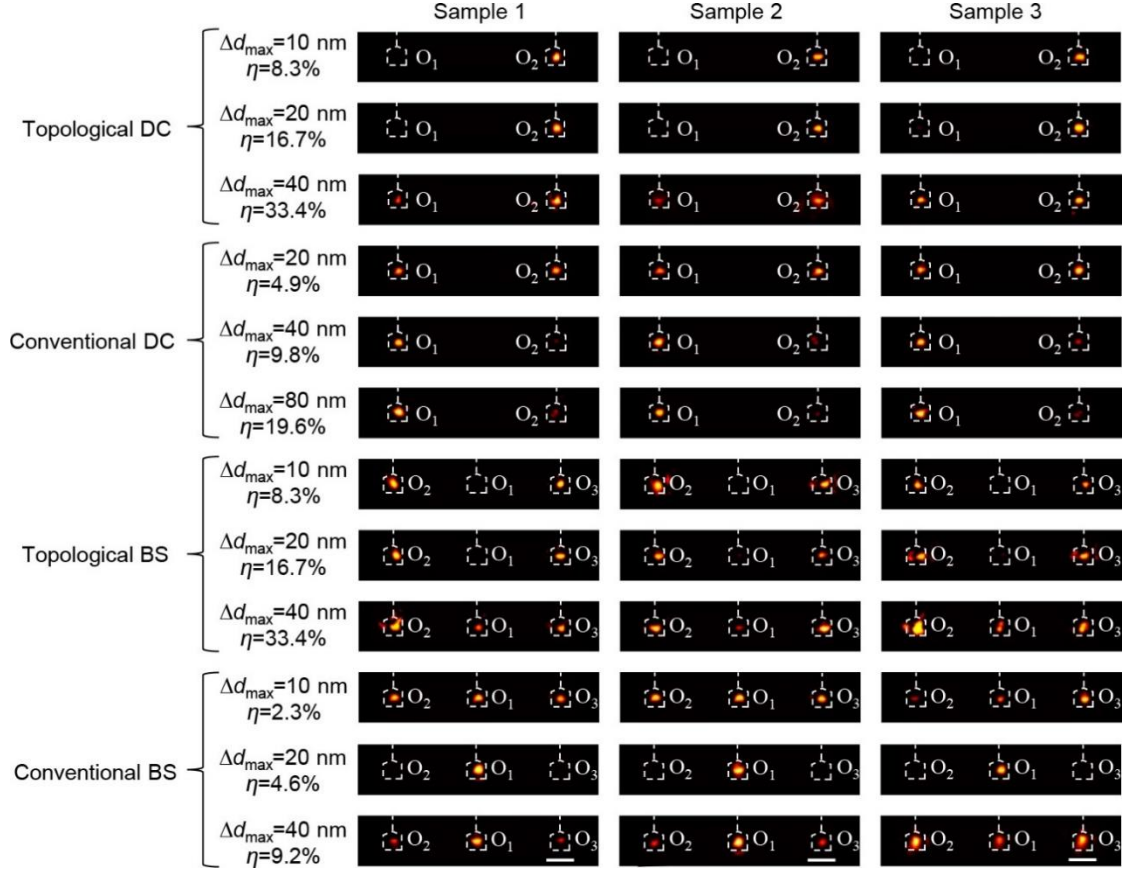


Figure S4. Detailed experimental results. Experimentally captured output signals of three different disordered topological DC, topological BS, conventional DC, and conventional BS devices with their deviation degree (η) and absolute disorders (Δd_{\max}) marked out. Scale bar=20 μm .

S3. The experimental results with exact input states

To realize the exact superposition states of coupled TESs, both the intensities and phases of the input state should be carefully prepared. By analyzing the model property of two TESs (see Figure 1h in the main text), we found that the optical field is mainly confined in the most-edge waveguide, with small amount in the third one. In our experiments, a branch arm split from main input waveguide was designed to connect to the third waveguide in the arrayed device. The detailed structural parameters are obtained by swapping in simulations to get a suitable mode profile matching to the

superposed TESs, which are provided in **Figure S5a**. Figure S5b,c show the simulation field and SEM image of input structure, respectively. Figure S5d shows the experimental directional coupling results with exactly prepared input mode, which shows very good DC performance as well. Similar design, simulation, and fabricated sample for the topological BS devices are displayed in Figure S5e-g, respectively. The experimental performances are given in Figure S5h, which also show relatively good BS function even for the large deviation $\eta=33.4\%$. By detailed analyses, it is found that the whole DC and BS performances are of the same level as the former single-waveguide input cases. As has been mentioned in the text, it mainly attributes to the fact that edge states have major field confinement in the single waveguide for these TESs. To simplify the manufacturing proceeding, we are reasonably in favor of the simple devices reported in the main text.

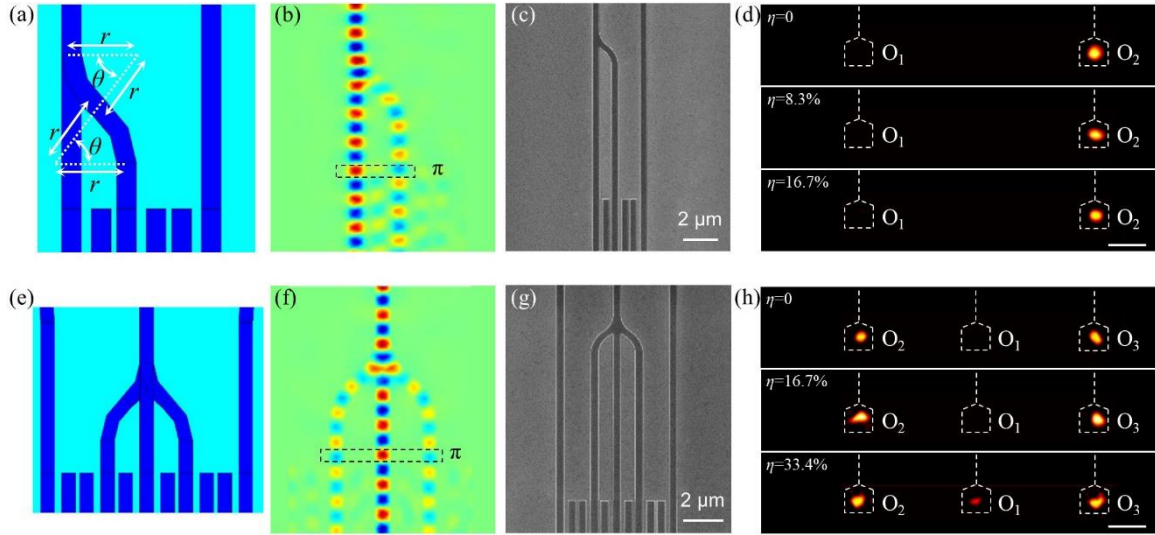


Figure S5. Input states control. (a) The design sketch of exact input superposed TES mode in topological DC device, where $r=1.384\ \mu\text{m}$ and $\vartheta=0.933\ \text{rad}$ after parameter optimization by simulations. (b) Simulation results of the field evolution in the designed input structures for the waveguide array, where a phase difference of π can be observed. (c) SEM image of the fabricated topological DC device with input state control. (d) Experimentally measured output intensities of the topological DC sample. Top: Ideal structures. Middle: Controlled structures with structural

discrepancy $\eta=8.3\%$ ($\Delta d_{\max}=10$ nm). Bottom: Controlled structures with structural discrepancy $\eta=16.7\%$ ($\Delta d_{\max}=20$ nm). The topological samples show almost unchanged localized field spots indicating robust optical coupling. (e-h) Corresponding design, simulation, SEM image, and BS performance for the topological BS device with exact input state. (h) Top: Ideal structures. Middle: Controlled structures with structural discrepancy $\eta=16.7\%$ ($\Delta d_{\max}=20$ nm). Bottom: Controlled structures with structural discrepancy $\eta=33.4\%$ ($\Delta d_{\max}=40$ nm). Scale bar = 20 μm .